



# Mechanical properties of the inertia friction welded aluminum/stainless steel joint

Yong Liu<sup>1,2</sup> · Haiyan Zhao<sup>1</sup> · Yun Peng<sup>2</sup> · Xiaofei Ma<sup>3</sup>

Received: 15 April 2019 / Accepted: 2 August 2019 / Published online: 17 August 2019  
© International Institute of Welding 2019

## Abstract

Mechanical properties of aluminum alloy/stainless steel joint including tensile strength, bending angle, impact toughness, and fatigue property were evaluated, and the effects of friction pressure and rotational speed were also discussed in this work. Results showed that the intermetallic compound (IMC) layer was formed at the bonding interface of the joint, and a thicker IMC layer was observed in the outer region of the joint, and the thickness decreased slightly in the edge region. The thickness of the IMC layer increased with increasing rotational speed. As friction pressure increased, the tensile strength of the joint gradually increased. Joint strength reached to the maximum tensile strength of 323 MPa when the rotational speed and friction pressure were 1100 rpm and 180 MPa, respectively. With the increase of friction pressure, the bending angle of the joint first increased and then decreased. The bending angle reached to 94°, and the welded joint had the excellent bending ductility. The average impact-absorbing energy of joints was 14.47 J, and the maximum fatigue cycle number of joints could reach to  $1.25 \times 10^5$ .

**Keywords** Inertia friction welding · Dissimilar welded joint · Tensile strength · Bending angle · Fatigue property · Fracture surface

## 1 Introduction

Hybrid structures of aluminum/stainless steel are of great interest for purposes of lightweight and corrosion protection, and have attracted much attention in industries including aerospace, electrical, automotive, agricultural, defense, and marine [1–7].

High welding quality of aluminum/steel joints is vital to ensure their applications. Many processes have been tried to weld aluminum alloy and stainless steel, such as fusion welding and solid-state welding [8–14]. The dissimilar metal of fusion welding has many difficulties: metallurgical incompatibility, formation of brittle phases, large residual stresses, and segregation of high- and low-melting phase [15]. Friction welding is a solid-state joining method and has extensively been used because of the advantages such as high material saving and low production time [16, 17]. Inertia friction welding, one of the friction welding, is a unique method of joining materials achieved by a hot-heavy working process. During welding, friction and plastic deformation generate heat at the interface and collapse surface asperities. The softened material is expelled from the interface to create nascent surfaces in close contact, and a high-quality bond between the two workpieces is formed consequently [18, 19]. In addition, inertia friction welding could limit the formation of intermetallic compound (IMC), which is suitable for the dissimilar joint due to lower heat input, short welding cycle, and less welding parameters [20].

Some researches on friction welding between aluminum alloy and stainless steel have been studied [21–23]. Kimura et al. clarified the joining mechanism during the friction

---

Recommended for publication by Commission III - Resistance Welding, Solid State Welding, and Allied Joining Process

---

- ✉ Yong Liu  
liuyong1350130711@126.com
- ✉ Haiyan Zhao  
hyzhao@tsinghua.edu.cn
- ✉ Yun Peng  
pengyun@cisri.com.cn

<sup>1</sup> School of Materials Science and Engineering, Tsinghua University, Beijing 100084, China  
<sup>2</sup> China Iron & Steel Research Institute Group, Beijing 100081, China  
<sup>3</sup> School of Materials Science and Engineering, Shandong University, Jinan 250061, China

welding process between commercially pure aluminum and 304 austenitic stainless steel, and the welded joint had the excellent bend ductility [24]. Luo et al. analyzed the microstructure and mechanical properties of steel/copper bimetallic joint, and the results showed that there was a friction interface–transferring phenomenon during welding [25]. Switznier et al. achieved joining between 304L stainless steel and AISI 1018 steel by inertia friction welding. They found that rotation speed and axial pressure were varied to determine the morphology, microstructure, and mechanical properties of the joint [26]. Dong et al. investigated the effect of post-weld heat treatment on the mechanical properties and microstructure of joints, and found that solid steel/titanium joint could be obtained without adding interlayer [27]. B. Grant et al. performed a numerical analysis of inertia friction welding of a sequentially coupled thermal-mechanical finite element model.

Friction welding is a complicated metallurgical process that is accompanied by frictional heat generation and plastic deformation. N. Rajesh et al. developed a finite element-based numerical model to understand the thermo-mechanical phenomenon involved in the process of friction welding [28]. However, previous studies have rarely used inertia friction welding technology to produce aluminum alloy/stainless steel joints, and there are few reports on the comprehensively mechanical properties of inertia friction welded joints. In this study, we focused on the evaluation of mechanical properties of welded joints including tensile strength, bending property, impact toughness, and fatigue property. The effects of friction pressure and rotational speed on the microstructure and mechanical properties of joints were studied.

## 2 Experimental procedure

### 2.1 Materials

Base metals were 6061-T6 aluminum alloy (Al 6061) and 304 stainless steel (SS 304) rods, and the rod diameter was 15 mm. The chemical composition of Al 6061 and SS 304 are listed in Table 1.

### 2.2 Inertia friction welding process

A modified HSMZ-4 inertia friction welding was used to join aluminum alloy and stainless steel. Before welding, the rod

**Table 1** The chemical compositions of Al 6061 and SS 304 (wt%)

Metal	Fe	Mg	Si	Mn	Cu	Cr	Zn	Ni	Al
Al 6061	0.73	1.02	0.69	0.13	0.20	0.10	0.28	0.05	Balance
SS 304	71.7	–	0.62	1.44	0.30	17.15	1.10	8.15	0.01

surface was polished by sandpapers and then cleaned by acetone. A stainless steel rod was fixed on the rotary jaw, and an aluminum alloy rod was fixed on the stationary jaw. When the spindle was accelerated to the predetermined rotational speed, the motor was cut off automatically. The stainless steel rod rotated at high revolutions with the spindle, and the aluminum alloy rod moved axially under the constant axial pressure. The connected surfaces rubbed together when base metals reached the plastic state. The rotational speed of the component with spindle slowed down gradually until the welding procedure was finished [20]. Experiments were performed three times for each set of parameters. Moment of inertia was 0.16 kg m<sup>2</sup>. The axial friction pressure ( $P_f$ ) was 140–220 MPa, and the rotational speed ( $n$ ) was 900–1500 rpm.

The thermal cycle acquisition system was used to record the welding temperature in real time. This system was mainly composed of thermocouple module, temperature acquisition control software, shielding chassis, and special cable [29]. A K-type thermocouple ( $\leq 1300$  °C) was used to collect the welding temperature data, and the temperature acquisition frequency was 1000 Hz, and its measurement accuracy was about  $\pm 2.5$  °C. In order to place thermocouples, small holes were drilled vertically at a distance of 0.5 mm from the Al 6061 side, and the drilling depth was 2.5 mm, 5 mm, and 7.5 mm from the surface, respectively, as shown in Fig. 1.

### 2.3 Characterization

Welding joints were cut by an electrical discharge machine, and then gradually ground and polished to observe microstructure. SS 304 (side) was etched by a solution (2.5 mL HNO<sub>3</sub> and 97.5 mL ethanol), and Al 6061 (side) was etched by Keller's reagent (1.0 mL HF, 1.5 mL HCl, 2.5 mL HNO<sub>3</sub>, and 95 mL H<sub>2</sub>O). The microstructure was observed by optical microscopy (OM) and field emission scanning electron microscope (SEM).

Tensile specimens were prepared based on GB/T228.1-2010. The tensile properties of joints were measured by a universal testing machine at a constant displacement rate of

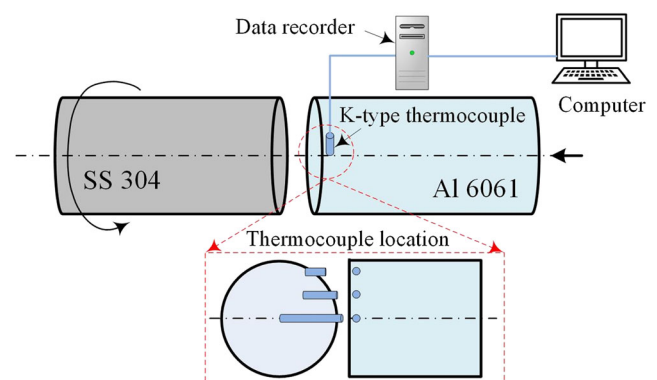
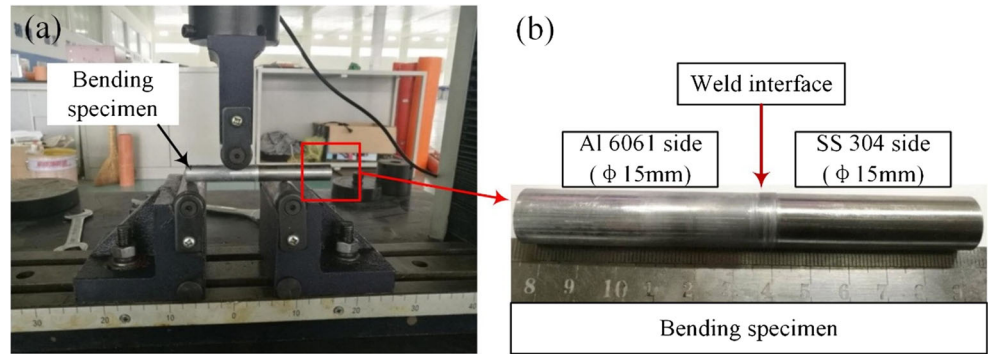


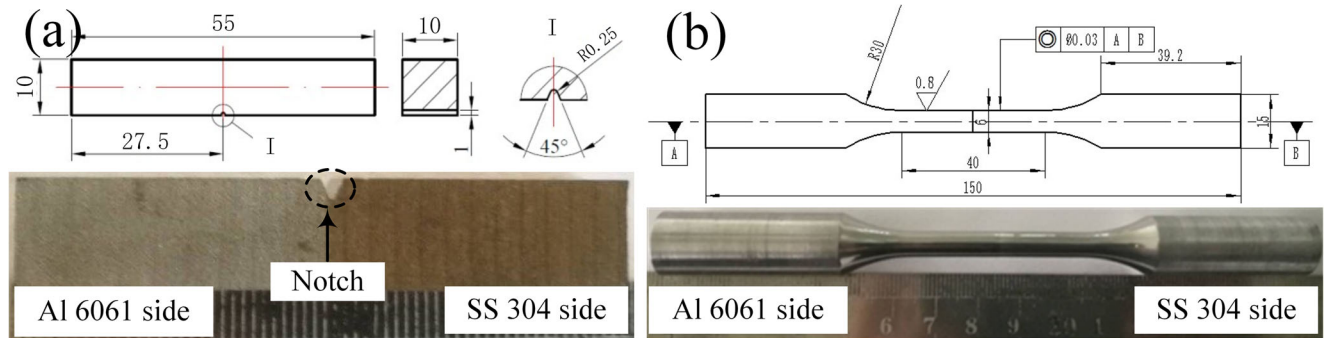
**Fig. 1** Arrangement of thermocouples during inertia friction welding

**Fig. 2** Bending properties of the welded joint: (a) test machine; (b) bending specimen



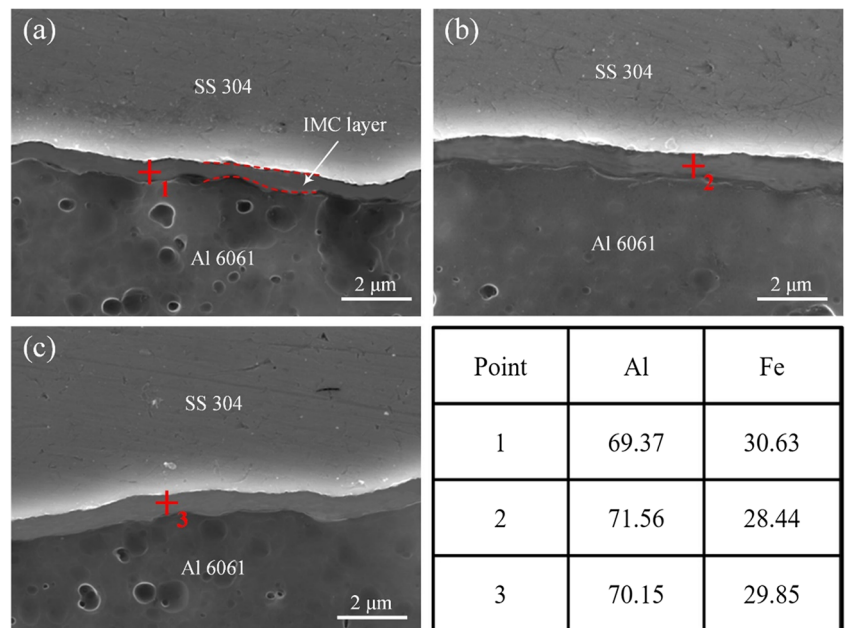
1 mm/min at room temperature. Tensile strength was calculated by dividing the ultimate shear tensile load by an area of 15-mm diameter. The average tensile strength was obtained from the three tensile specimens. Bending specimens were prepared based on the JIIS Z2248:2006. The bending properties were measured by a universal testing machine at a constant bending speed of 2 mm/min at room temperature, as shown in Fig. 2.

In order to evaluate the plastic toughness of joint, standard specimens were prepared according to the GB/T 2650-2008. The position of the notch was located at the bonding interface. The dimension of impact specimen is shown in Fig. 3a. Fatigue specimens were prepared according to the metal fatigue test standard GB/T 3075-2008. The dimension of the fatigue specimen is shown in Fig. 3b. The specimen surface



**Fig. 3** a The dimension of impact specimens. b The dimension of tensile fatigue specimens (mm)

**Fig. 4** SEM images of welding interface at different positions ( $P_f=180$  MPa,  $n=1100$  rpm). a The center. b The 1/2 radius. c The edge. The composition of measured points (at%)



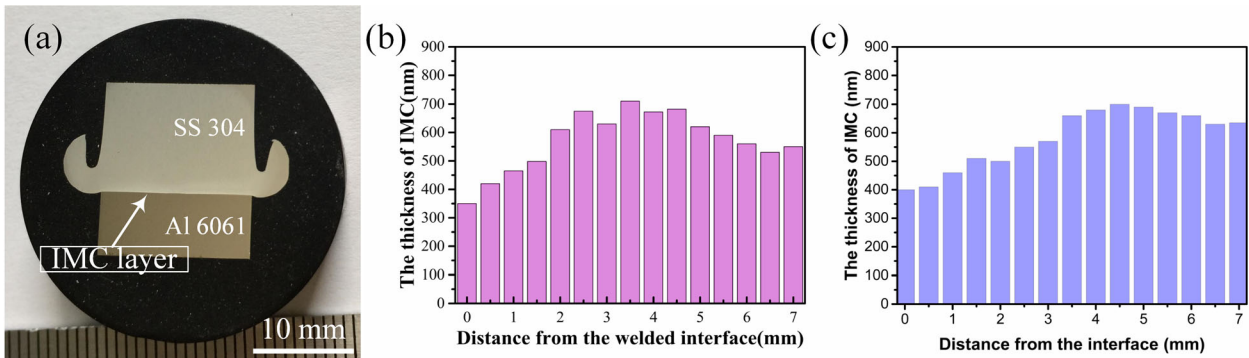


**Fig. 5** **a** Macrographs of the cross-section of joints, and distribution of IMC thickness at the interface of joint. **b**  $P_f = 180$  MPa,  $n = 1100$  rpm. **c**  $P_f = 180$  MPa,  $n = 1300$  rpm

was ground to eliminate the effect of stress concentration. These fracture surface after the test was characterized by the SEM and X-ray diffractometer (XRD).

### 3 Results and discussion

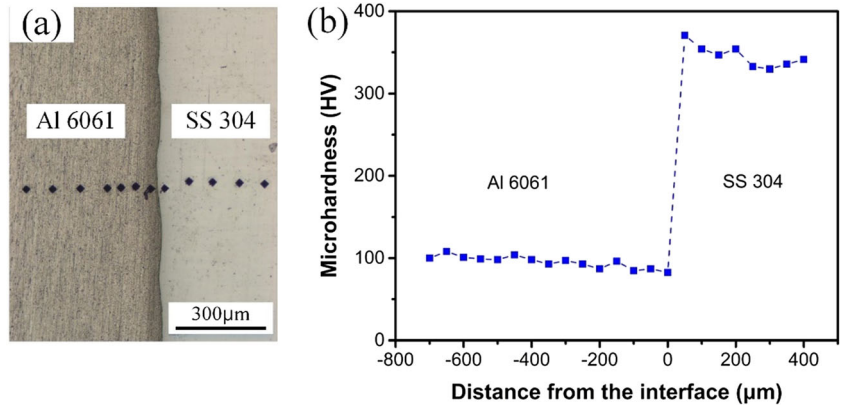
#### 3.1 Microstructure of joint

The stored kinetic energy could be released in a short time during inertia friction welding and promoted the diffusion of Al and Fe atoms at the interface [30]. Diffusion eventually

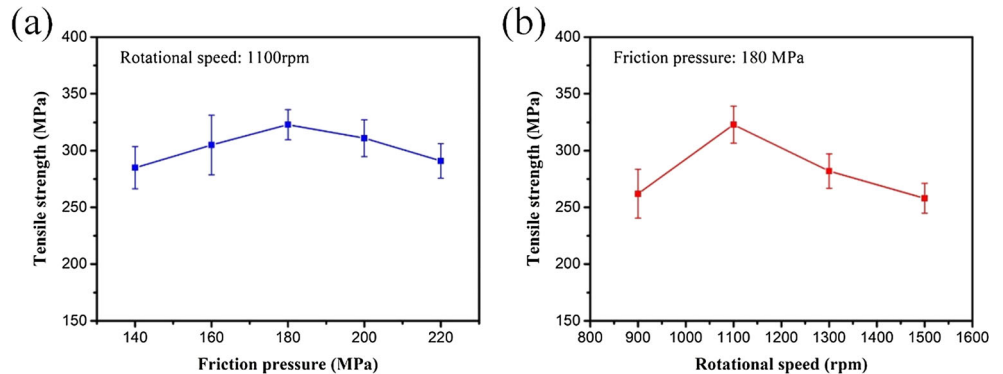
achieved the atom-atom metallurgical bonding and formed the IMC layer. The formation of IMC at the bonding interface was inevitable due to the limited solubility of Fe and Al [31]. The thickness of the IMC layer was measured by SEM images. The Al/Fe joint was welded at 180 MPa and 1100 rpm, and the distribution and thickness of the IMC layer at the interface are shown in Fig. 4. Based on the EDS results, the IMC layer should contain  $Fe_2Al_5$  phase, which has a very high hardness and low fracture toughness [32–34].

The thickness of the IMC layer was not the same at different positions. A thicker IMC layer was usually observed in the outer region, and the thickness decreased slightly in the

**Fig. 6** **a** Optical image of the cross-section of the joint. **b** Microhardness distribution ( $n = 1100$  rpm,  $P_f = 180$  MPa)



**Fig. 7** Influence of process parameters on the tensile strength of the joint. **a** Friction pressure ( $n = 1100$  rpm). **b** Rotational speed ( $P_f = 180$  MPa)



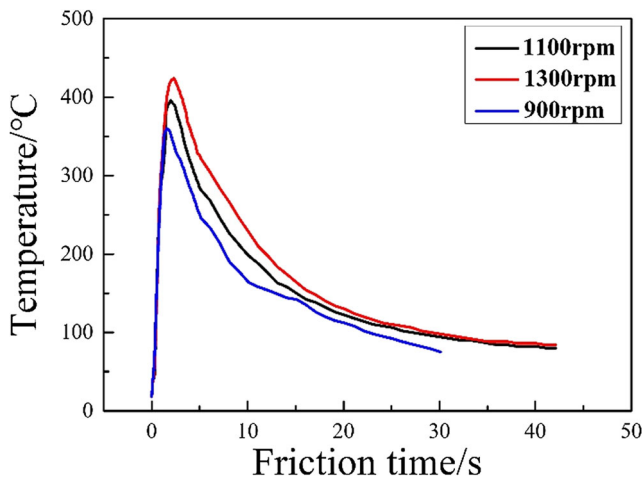


**Fig. 8** Temperament profile during friction welding ( $P_f = 180$  MPa)

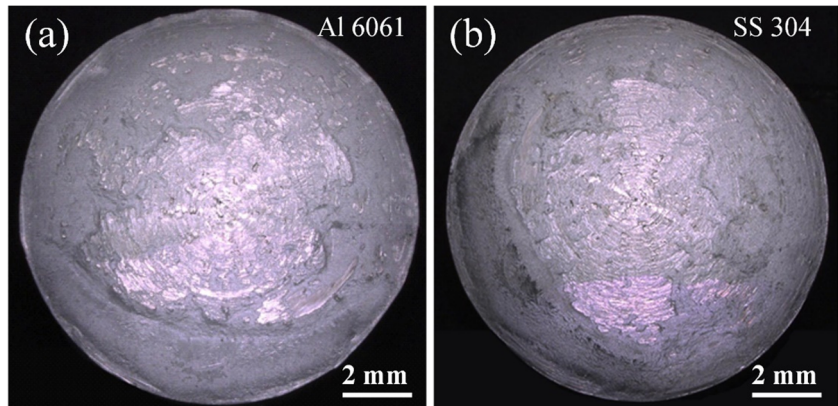
outermost region (edge region), as shown in Fig. 5. The reason should be that the outer region experienced a stronger thermo-

mechanical effect than the center region. The decrease in thickness in the outermost region was a result of the expulsion of the flash. The average thickness of the IMC layer was about 600 nm. A thick IMC layer was the primary source for producing weak joining and the control of IMC thickness was the key to success in producing reliable joints [35].

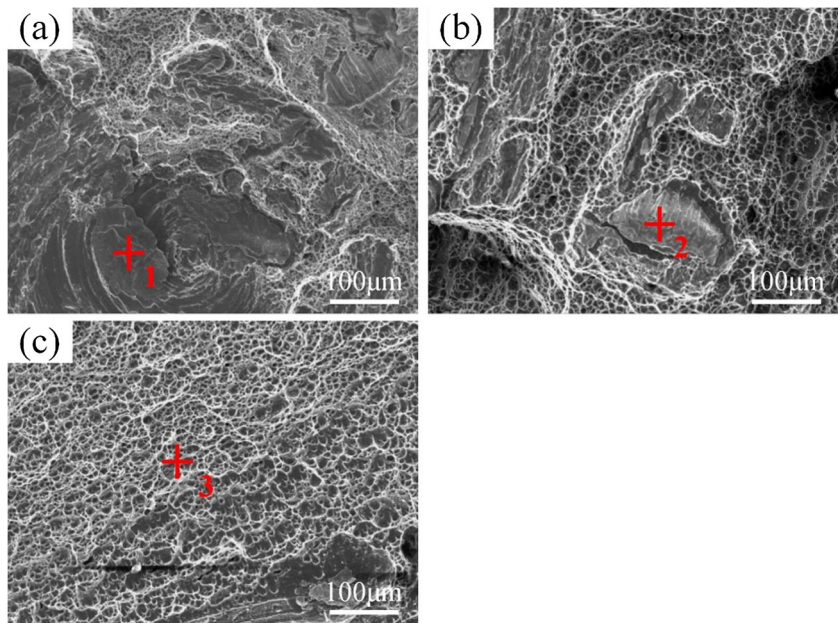
The thickness of the IMC layer increased with the rotational speed, as shown in Fig. 5b, c. The IMC layer thickness and distribution corresponded to the temperature distribution. It was important to determine the critical thickness regarding whether the joint fractured at the bonding interface, and S. Fukumoto thought that the critical thickness was about 700 nm [36].

Figure 6 shows the microhardness distribution across the joint. Hardening was observed on the SS 304 side of the interface, and the maximum hardness level was about 370 Hv. The reason should be that high plastic deformation caused a strong decrease in grain size and the formation of a hard IMC

**Fig. 9** Fracture morphology of joint after the tensile test. **a** Al 6061 side. **b** SS 304 side ( $P_f = 180$  MPa,  $n = 1100$  rpm)



**Fig. 10** Fracture surface on the stainless steel side. **a** The center region. **b** The 1/2 radius region. **c** The edge region ( $P_f = 180$  MPa,  $n = 1100$  rpm)



**Table 2** The composition of position in Fig. 9 (at%)

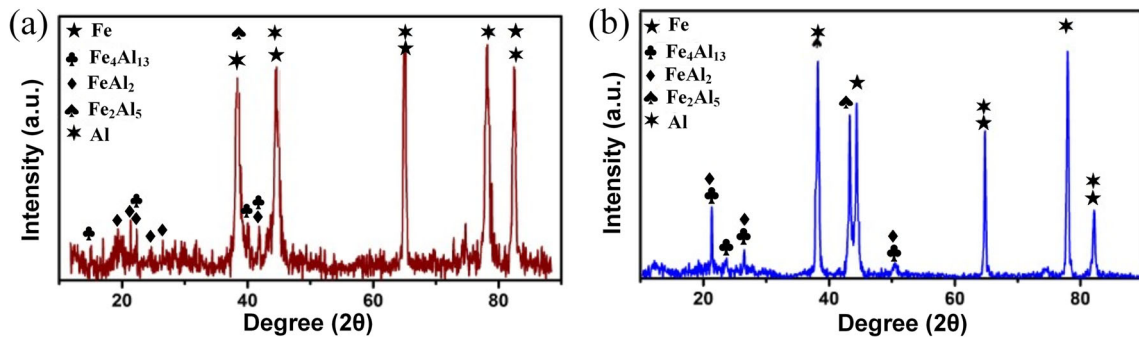
Position	Al	Fe
1	68.32	31.68
2	71.40	28.60
3	99.12	0.88

layer, which led to hardening in the region of the interface. The increase in the hardness of the stainless steel near the interface could be related directly to the high deformation hardening in austenitic steels in general [37].

### 3.2 Tensile property of joint

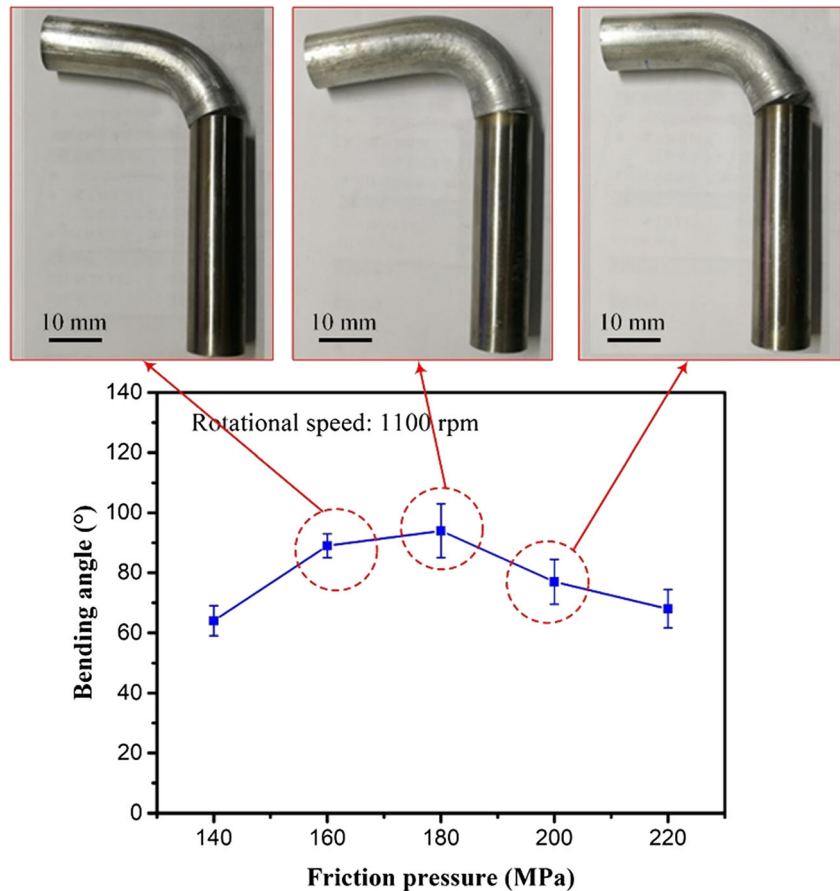
#### 3.2.1 Tensile strength

Figure 7 a shows the tensile strength of dissimilar joint as a function of friction pressure. As the friction pressure increased, tensile strength gradually increased. When the rotational speed was 1100 rpm and friction pressure was 180 MPa, the tensile strength of joint reached to the maximum tensile strength of 323 MPa, which was about 94% of Al 6061. If friction pressure continued to increase, joint strength started to decrease gradually.

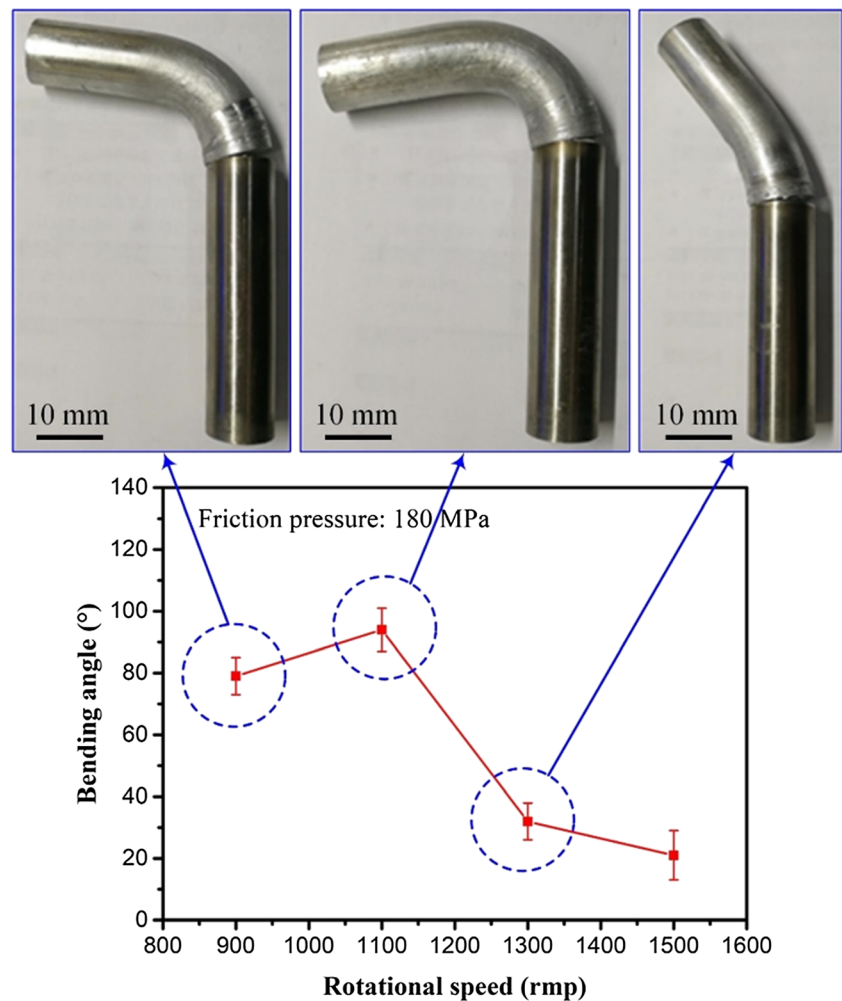


**Fig. 11** XRD patterns of the fracture surface. **a** Al 6061 side. **b** SS 304 side

**Fig. 12** Effect of friction pressure on the bending angle and morphology (*n* = 1100 rpm)



**Fig. 13** Effect of rotational speed on the bending angle ( $P_f = 180$  MPa)



Compared with the friction pressure, rotational speed had a more significant influence on the tensile strength, as shown in Fig. 7b, because welding heat input was mainly determined by the rotational speed of a flywheel. When the rotational speed increased from 900 to 1300 rpm, the frictional heat generated at the aluminum/steel interface also increased rapidly, as shown in Fig. 8. The rapid rise of temperature resulted to plastic deformation on the aluminum side, and the fluidity of plastic metal also enhanced. Friction interface would be extruded along the radial direction of a joint under a certain axial pressure, and the deformed metal would transition into the flash. The tensile strength changed with the rotational speed. When the rotational speed was 1100 rpm, the joint reached to the maximum tensile strength of 323 MPa.

### 3.2.2 Fracture surface

Figure 9 shows the fracture surface of the joint after the tensile test. The fracture surface was rough and its color was silver-gray. The stainless steel side was almost covered by the aluminum matrix, and the aluminum alloy side occurred to the obvious

plastic deformation. These results indicated that the fracture initiated the heat affect zone, not the bonding interface.

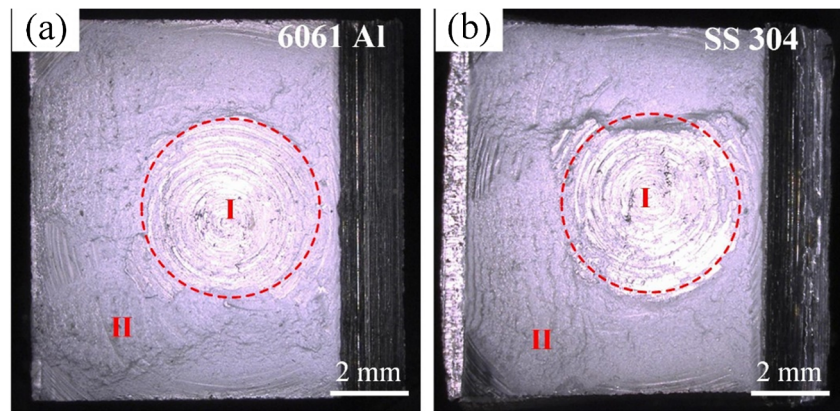
Figure 10 shows the SEM images of the fracture surface on the stainless steel side. Based on the EDS results (Table 2), the center of the fracture surface had many tearing ridges, which were mainly related to the formation of IMC, as shown in Fig. 8a. A large number of dimples distributed the entire fracture surface, indicating that the welded joint achieved metallurgical bonding (Fig. 10b, c).

The phase composition of the fracture surface was measured by XRD (Fig. 11). Al,  $Fe_2Al_5$ ,  $Fe_4Al_{13}$ , and Fe phases

**Table 3** Results of impact test for the joint and base metals

Specimens	Impact-absorbing energy (J)
The welded joint	16.14
	14.73
	15.56
6061Al base metal	19.64
SS 304 base metal	100.69

**Fig. 14** Fracture morphology of joint after impact test ( $P_f=180$  MPa,  $n=1100$  rpm). **a** Al 6061 side. **b** SS 304 side



were detected on both the fracture surfaces. The presence of IMC confirmed the joint had formed the metallurgical bonding. However, many brittle and hard phases would also weaken the strength of the joint.

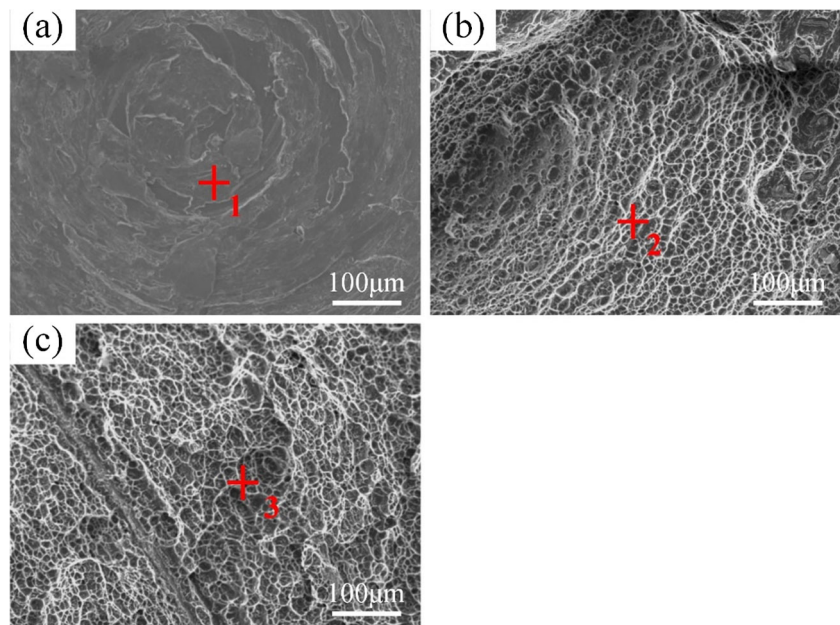
### 3.3 Bending property of joint

Figure 12 shows the effect of process parameter on the bending angle of the joint. With the increase of friction pressure, the bending angle first increased and then decreased. When friction pressure was 140 MPa, the bending angle was only  $64^\circ$ . When the friction pressure was 180 MPa, the bending

The inner side of the joint was affected by the tensile stress, and a large number of dislocations moved along the slip surface. The bonding interface was the stress concentration region, and the outside of the joint was elongated due to the large tensile stress and cracked.

With the increase of rotational speed, the bending angle first increased and then decreased, as shown in Fig. 13. When joints were made with a friction pressure of 180 MPa and rotational speed of 1100 rpm, the bending angle reached to the maximum value and joints had the bend ductility of  $90^\circ$  with no crack at the bonding interface. Therefore, the sound joints were achieved and satisfied with the superlative grade of

**Fig. 15** SEM images of fracture surface after impact test. **a** The center of the fracture surface. **b** 1/2 radius position. **c** The edge of fracture surface



angle reached to the maximum value of  $94^\circ$ . When the bending angle was beyond  $90^\circ$ , the joint had the sound bonding interface and excellent bending ductility. After bending, the aluminum alloy side of joint had obvious plastic deformation, while the stainless steel side did not occur to the deformation.

**Table 4** The composition of position in Fig. 14 (at%)

Position	Al	Fe
1	65.49	34.51
2	3.22	96.78
3	97.32	2.68



**Table 5** Axial tensile fatigue test results of joint

Samples	Fatigue cycles	Failure position
1	$8.8797 \times 10^4$	Welding interface
2	$1.1671 \times 10^5$	Welding interface
3	$1.25078 \times 10^5$	Welding interface

the classification of quality for friction welded joints on dissimilar metallic materials in JIS Z3175a. In addition, it was worth noting that the bend ductility of the joint was related to the bending force and bonding interface.

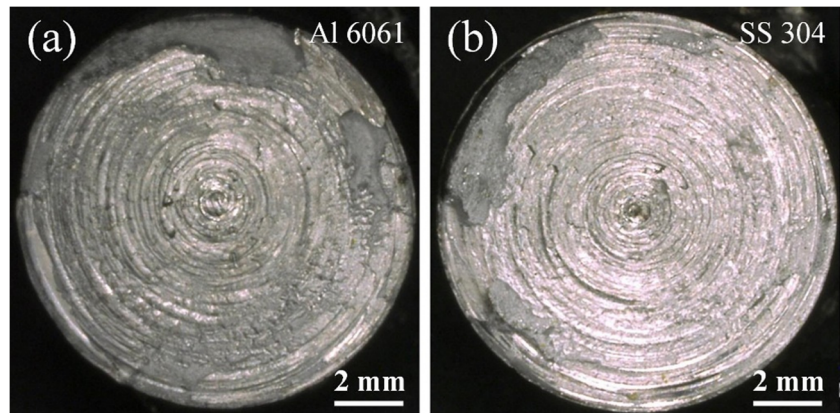
### 3.4 Impact property of joint

Impact strength of the joint was evaluated by the impact test. Based on the impact strength results (Table 3), the average impact absorbing the energy of joint was 14.47 J, which was

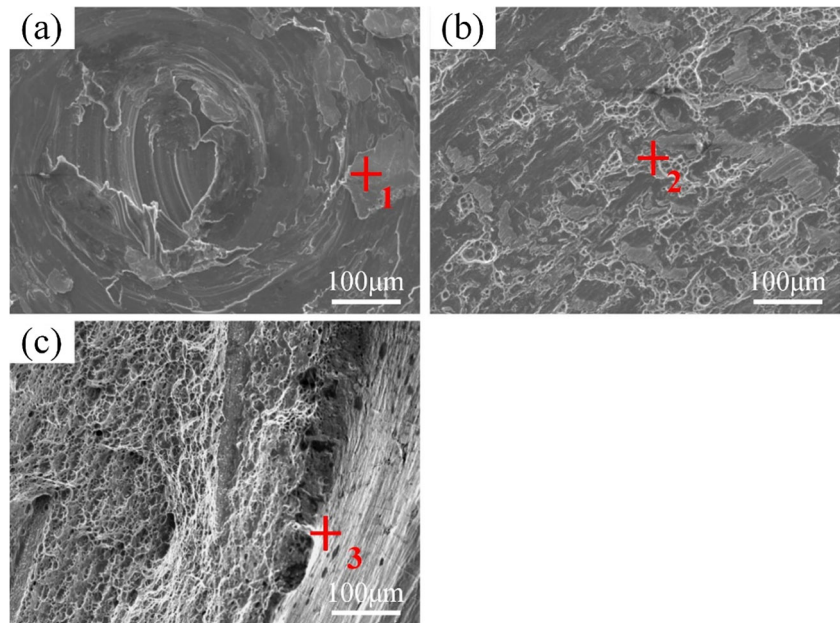
about 82% of Al 6061. The impact property of the dissimilar joint was determined by both metal properties. During friction welding, metal surfaces underwent both heat and force, and formed the metallurgical bonding. However, the brittle and hard IMC led to a decrease of impact toughness. Sufficiently metallurgical bonding could guarantee the good static tensile strength, while the IMC reduced the plastic toughness, making it difficult to obtain higher impact strength than base metals.

Figure 14 shows the fracture surface of the specimen after the impact test. The fracture surface consisted of two obvious regions (marked region I and II). Region I was the center of a fracture surface and relatively flat. Only a small number of IMC were detected, indicating that the metallurgical bonding in this region was limited (Fig. 14a). Region II contained many dimples and lamellar structure, and EDS results indicated that the local failure position was base metal (Fig. 15b–c, Table 4). Under the dynamic load condition, cracks were easy to initiate from the region I and expand.

**Fig. 16** Fracture morphology of joint after tensile fatigue test ( $P_f = 180$  MPa,  $n = 1100$  rpm). **a** Al 6061 side. **b** SS 304 side



**Fig. 17** SEM images of fracture surface after tensile fatigue test. **a** The center of fracture surface. **b** 1/2 radius position. **c** The edge of fracture surface



**Table 6** The composition of position in Fig. 12 (at%)

Position	Al	Fe
1	73.06	26.94
2	68.83	31.17
3	96.33	3.67

### 3.5 Fatigue property of joint

Combined with the actual force of the welded joint, the stress level was  $0.6\sigma_b=192$  MPa and the stress ratio was 0.1. The applied direction of the load was perpendicular to the welded joint, and the alternating load frequency was 10 Hz. Table 5 shows the results of the low-frequency fatigue results of the joint. The maximum number of fatigue cycle reached  $1.25 \times 10^5$ , which could satisfy the practical application of joint.

Under the continuous load, the welded joint would first generate cracks at the high-stress position, and then cracks expanded. All specimens failed at the bonding interfaces. There was a ring-shaped tear mark on the fracture surface, and the crack initiation portion was perpendicular to the central region of the tear ring, as shown in Fig. 16. By observing SEM images of the fracture surface on the stainless steel side, there were sheet-like IMC on the fracture surface, which should be related to the fracture position (Fig. 17; Table 6).

## 4 Conclusions

1. The IMC layer was formed at the bonding interface of the joint. The thicker IMC layer was observed in the outer region, and the thickness decreased slightly in the edge region. The thickness of an IMC layer increased with rotational speed.
2. As friction pressure increased, the tensile strength of the joint gradually increased. Compared with the friction pressure, rotational speed had a more significant influence on the tensile strength. When the rotational speed was 1100 rpm and the friction pressure was 180 MPa, joint strength reached to the maximum tensile strength of 323 MPa.
3. With the increase of friction pressure, the bending angle first increased and then decreased. When the friction pressure was 180 MPa, the bending angle reached to the maximum value of  $94^\circ$ , and the welded joint had the excellent bending ductility.
4. The average impact absorbing the energy of joint was 14.47 J, and the maximum fatigue cycle of joint could reach to  $1.25 \times 10^5$ .

## References

1. Wan L, Huang Y (2018) Friction welding of AA6061 to AISI 316L steel: characteristic analysis and novel design equipment. *Int J Adv Manuf Technol* 95:4117–4128
2. Wang T, Sidhar H, Mishra RS, Hovanski Y, Upadhyay P, Carlson B (2018) Friction stir scribe welding technique for dissimilar joining of aluminium and galvanised steel. *Sci Technol Weld Join* 23:249–255
3. Su S, Chen S, Mao Y, Xiao J, Vivek A, Daehn G (2019) Joining aluminium alloy 5A06 to stainless steel 321 by vaporizing foil actuators welding with an interlayer. *Metals* 9:1–11
4. Zhang W, Sun D, Han L, Li Y (2015) Optimised design of electrode morphology for novel dissimilar resistance spot welding of aluminium alloy and galvanised high strength steel. *Mater Des* 85:461–470
5. Su Y, Hua X, Wu Y (2014) Influence of alloy elements on microstructure and mechanical property of aluminum–steel lap joint made by gas metal arc welding. *J Mater Process Technol* 214:750–755
6. Hincapié OD, Salazar JA, Restrepo JJ, Torres EA, Graciano-Urbe J (2019) Control of formation of intermetallic compound in dissimilar joints aluminum-steel. *Int J Eng Sci* 32:127–136
7. Ling Z, Li Y, Luo Z, Ao S, Yin Z, Gu Y, Chen Q (2017) Microstructure and fatigue behavior of resistance element welded dissimilar joints of DP780 dual-phase steel to 6061-T6 aluminum alloy. *Int J Adv Manuf Technol* 92:1923–1931
8. Ogawa D, Kakiuchi T, Hashiba K, Uematsu Y (2019) Residual stress measurement of Al/steel dissimilar friction stir weld. *Sci Technol Weld Join* 1–10
9. Shen Z, Chen J, Ding Y, Hou J, Shalchi Amirkhiz B, Chan K, Gerlich AP (2018) Role of interfacial reaction on the mechanical performance of Al/steel dissimilar refill friction stir spot welds. *Sci Technol Weld Join* 23:462–477
10. Nguyen NV, Nguyen MQ, Huang S-C (2018) Microstructure and mechanical properties of butt joints between stainless steel SUS304L and aluminum alloy A6061-T6 by TIG welding. *Materials* 11:1–13
11. Li J, Li H, Wei H, Gao Y (2016) Effect of torch position and angle on welding quality and welding process stability in Pulse on Pulse MIG welding-brazing of aluminum alloy to stainless steel. *Int J Adv Manuf Technol* 84:705–716
12. Qin G, Su Y, Meng X, Fu B (2015) Numerical simulation on MIG arc brazing-fusion welding of aluminum alloy to galvanized steel plate. *Int J Adv Manuf Technol* 78:1917–1925
13. Sierra G, Peyre P, Deschaux Beaume F, Stuart D, Fras G (2008) Galvanised steel to aluminium joining by laser and GTAW processes. *Mater Charact* 59:1705–1715
14. Dong H, Li Y, Li P, Hao X, Xia Y, Yang G (2019) Inhomogeneous microstructure and mechanical properties of rotary friction welded joints between 5052 aluminum alloy and 304 stainless steel. *J Mater Process Technol* 272:17–27
15. Jafarian M, Khodabandeh A, Manafi S (2015) Evaluation of diffusion welding of 6061 aluminum and AZ31 magnesium alloys without using an interlayer. *Mater Des* 65:160–164
16. Sahin M (2007) Evaluation of the joint-interface properties of austenitic-stainless steels (AISI 304) joined by friction welding. *Mater Des* 28:2244–2250
17. Nicholas ED (2003) Friction Processing Technologies. *Weld World* 47:2–9
18. Tung DJ, Mahaffey DW, Senkov ON, Semiatin SL, Zhang W (2019) Transient behaviour of torque and process efficiency during inertia friction welding. *Sci Technol Weld Join* 24:136–147

19. Tiley JS, Mahaffey DW, Alam T, Rojhirunsakool T, Senkov O, Parthasarthy T, Banerjee R (2016) Strengthening mechanisms in an inertia friction welded nickel-base superalloy. *Mater Sci Eng A* 662:26–35
20. Guo W, You G, Yuan G, Zhang X (2017) Microstructure and mechanical properties of dissimilar inertia friction welding of 7A04 aluminum alloy to AZ31 magnesium alloy. *J Alloys Compd* 695:3267–3277
21. Reddy MG, Rao SA, Mohandas T (2008) Role of electroplated interlayer in continuous drive friction welding of AA6061 to AISI 304 dissimilar metals. *Sci Technol Weld Join* 13:619–628
22. Paventhan R, Lakshminarayanan PR, Balasubramanian V (2011) Prediction and optimization of friction welding parameters for joining aluminium alloy and stainless steel. *T Nonferrous Metal Soc* 21:1480–1485
23. Seli H, Ismail AIM, Rachman E, Ahmad ZA (2010) Mechanical evaluation and thermal modelling of friction welding of mild steel and aluminium. *J Mater Process Technol* 210:1209–1216
24. Kimura M, Suzuki K, Kusaka M, Kaizu K (2017) Effect of friction welding condition on joining phenomena, tensile strength, and bend ductility of friction welded joint between pure aluminium and AISI 304 stainless steel. *J Manuf Process* 25:116–125
25. Luo J, Liu S, Chen W, Xu X (2016) Friction interface migration of copper alloy and carbon steel dissimilar metal joints in inertia radial friction welding. *Mater Manuf Process* 31:275–282
26. Switzner N, Yu Z, Eff M, Lienert T, Fonseca A (2018) Microstructure and mechanical property variations within inertia friction-welded joints of stainless steel to steel. *Int J Adv Manuf Technol* 95:4327–4340
27. Dong H, Yu L, Deng D, Zhou W, Dong C (2015) Direct friction welding of TiAl alloy to 42CrMo steel rods. *Mater Manuf Process* 30:1104–1108
28. Hynes NRJ, Velu PS (2017) Simulation of friction welding of alumina and steel with aluminum interlayer. *Int J Adv Manuf Technol* 93:121–127
29. Liang Z, Qin G, Wang L, Meng X, Li F (2015) Microstructural characterization and mechanical properties of dissimilar friction welding of 1060 aluminum to AZ31B magnesium alloy. *Mater Sci Eng A* 645:170–180
30. Rathod M, Kutsuna M (2004) Joining of aluminum alloy 5052 and low-carbon steel by laser roll welding. *Weld J* 83:16-S
31. Li X, Scherf A, Heilmaier M, Stein F (2016) The Al-rich part of the Fe-Al phase diagram. *J Phase Equilib Diffus* 37:162–173
32. Hussein SA, Tahir ASM, Hadzley A (2015) Characteristics of aluminum-to-steel joint made by friction stir welding: a review. *Mater Today Commun* 5:32–49
33. Matysik P, Józwiak S, Czujko T (2015) Characterization of low-symmetry structures from phase equilibrium of Fe-Al system microstructures and mechanical properties. *Materials* 8:915–931
34. Yasuyama M, Ogawa K, Taka T (1996) Spot welding of aluminium and steel sheet with an insert of aluminium clad steel sheet: dissimilar metal joining of aluminium and steel sheet (1st report). *Weld Int* 10:963–970
35. Pouranvari M (2017) Critical assessment 27: dissimilar resistance spot welding of aluminium/steel: challenges and opportunities. *Mater Sci Technol* 33:1705–1712
36. Fukumoto S, Tsubakino H, Okita K, Aritoshi M, Tomita T (1999) Friction welding process of 5052 aluminium alloy to 304 stainless steel. *Mater Sci Technol* 15:1080–1086
37. Yılmaz M, Çöl M, Acet M (2003) Interface properties of aluminum/steel friction-welded components. *Mater Charact* 49:421–429

**Publisher's note** Springer Nature remains neutral with regard to jurisdictional claims in published maps and institutional affiliations.